Electronic Supplementary Information

Highly Robust and Efficient Dye Rejection Enabled by rGO/MXene Heterogeneous Membranes

Rujie Yang [a,b], Pengxu Wang[a], Liuyuan Zhu[a], Yingjie Di[a], Yingying Huang[a]*, Binjie Zhou[a], Shujin Wu[c], Haiping Fang[a.b], and Shanshan Liang [a,c,d]*

[a]School of Physics, East China University of Science and Technology, Shanghai, China, 200237

[b]National Engineering Research Center of Industrial Wastewater Detoxication and Resource Recovery, East China University of Science and Technology, Shanghai, 200237, China

[C]China University of Petroleum-Beijing at Karamay, Karamay, Xinjiang, 834000, China

[d]State Key Laboratory of Chemical Engineering and Low-Carbon Technology, School of Chemical Engineering, East China University of Science and Technology, 130 Meilong Road, Shanghai 200237, China

Email: liangshanshan@ecust.edu.cn and huangyingying@ecust.edu.cn

Contents

PS. 1 Computational methods

Density functional theory (DFT) calculations were performed using the Vienna ab initio Simulation Package (VASP) code [S1]. Projector augmented wave (PAW) pseudopotentials were employed [S2], and the exchange-correlation interactions were treated within the generalized gradient approximation (GGA) using the Perdew-Burke-Ernzerhof (PBE) functional [S3]. To accurately describe the weak interactions, the van der Waals (vdW) corrections were introduced in the calculations through Grimme's D-3 method [S4]. The plane-wave cutoff energy was set to 600 eV. The Brillouin zones were sampled using a Gamma centered 3 × 3 × 1 k-point mesh [S5]. To eliminate spurious interactions between periodic images, a vacuum space of 30 Å was used along the z-direction. The geometry structures were fully relaxed until the residual force on each atom was less than 0.01 eV $Å^{-1}$, and the energy convergence criterion was set to 10^{-4} eV.

The adsorption energy (E_{ads}) was defined as $E_{ads} = E_{H_2O@slab} - E_{slab} - E_{H_2O}$, where $E_{H_2O@slab}$ is the total energy of the system with the water molecule adsorbed on the slab, E_{slab} is the energy of the slab (rGO and MXene), and E_{H_2O} is the energy of the isolated H_2O molecule.

PS. 2 The Tyndall effect of the rGO/MXene precursor solutions.

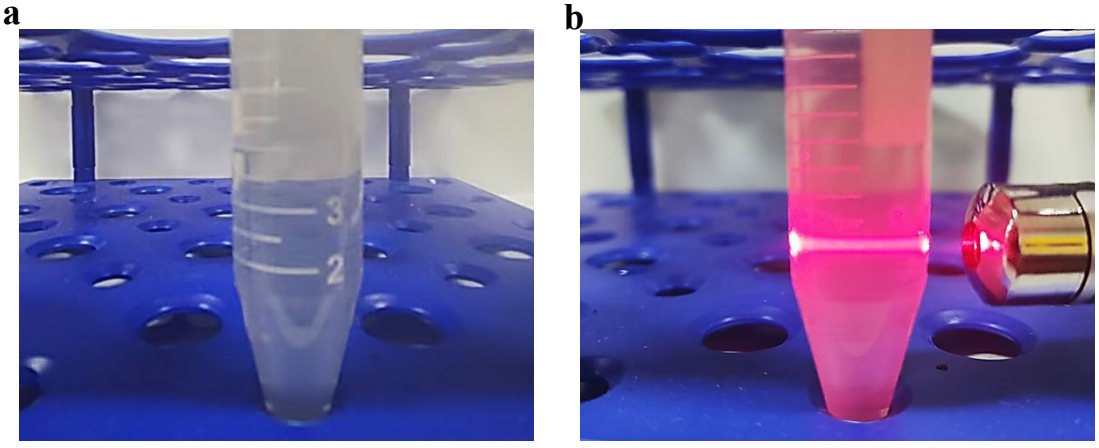

Fig. S1. (a) The post-dilution of the rGO/MXene precursor solutions. (b) The Tyndall effect of the rGO/MXene precursor solutions.

PS. 3 HAADF-STEM imaging combined with EELS spectrum mapping

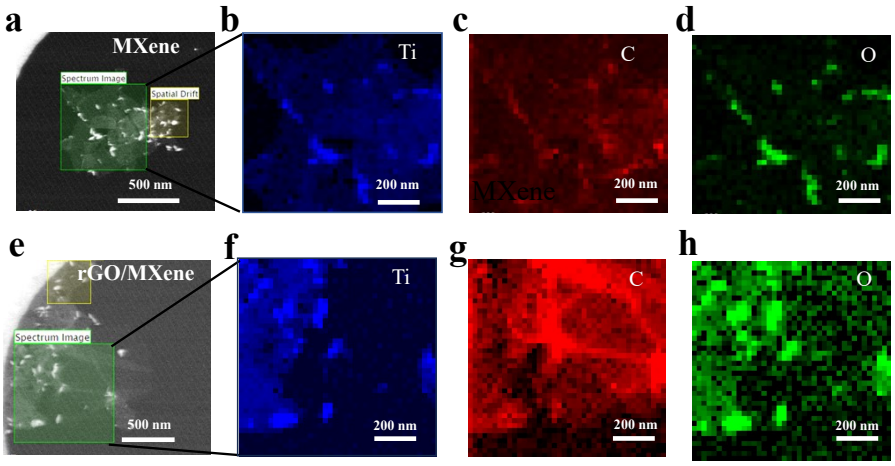

Fig. S2. HAADF-STEM imaging combined with EELS spectrum mapping. (a) HAADF image, maps of (b) Titanium ,(c) Carbon and (d) Oxygen EELS K-edge integrated signals derived from the spectrum image of MXene nanosheet. (e) HAADF image, maps of (f) Titanium ,(g) Carbon and (h) Oxygen EELS K-edge integrated signals derived from the spectrum image of rGO/MXene nanosheet.

PS. 4 AFM images of rGO and rGO/MXene heterogeneous membranes

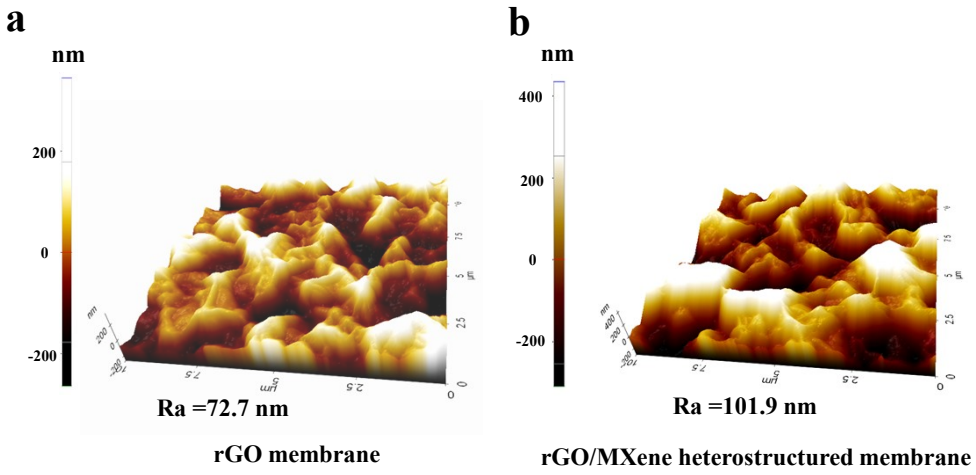

Fig. S3. AFM images of rGO and rGO/MXene heterogeneous membranes on silica substrates, respectively.

PS. 5 The water contact angles of the rGO and rGO/MXene heterogeneous membrane

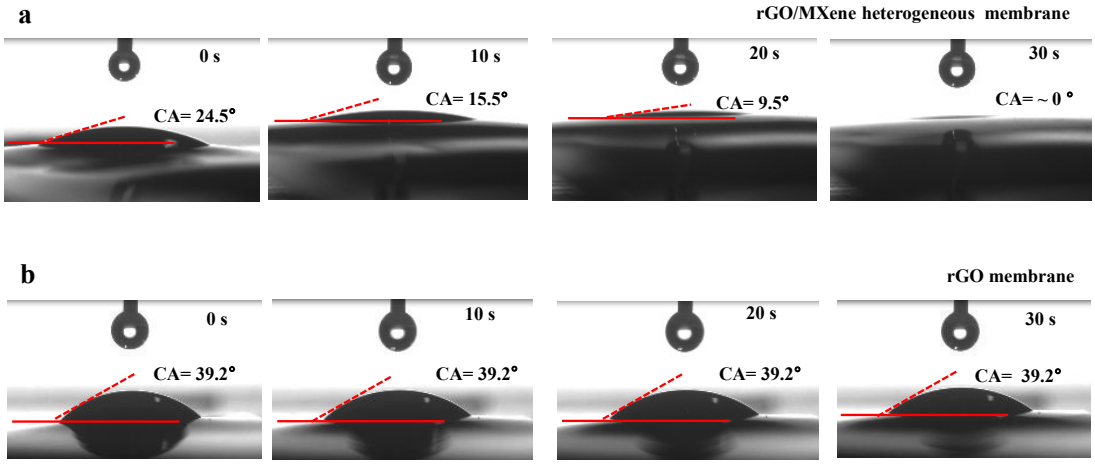

Fig. S4. The water contact angles of the rGO and rGO/MXene heterogeneous membranes with time.

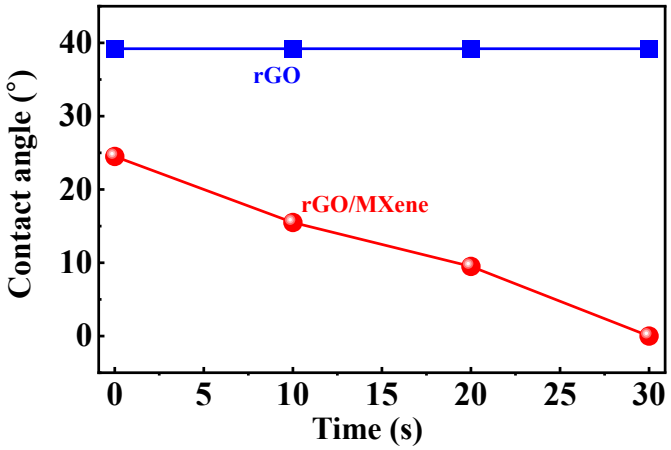

Fig. S5. The dynamic wetting curve of the rGO and rGO/MXene heterogeneous membranes with time.

PS. 6 XPS spectra of the rGO and rGO/MXene heterogeneous membranes

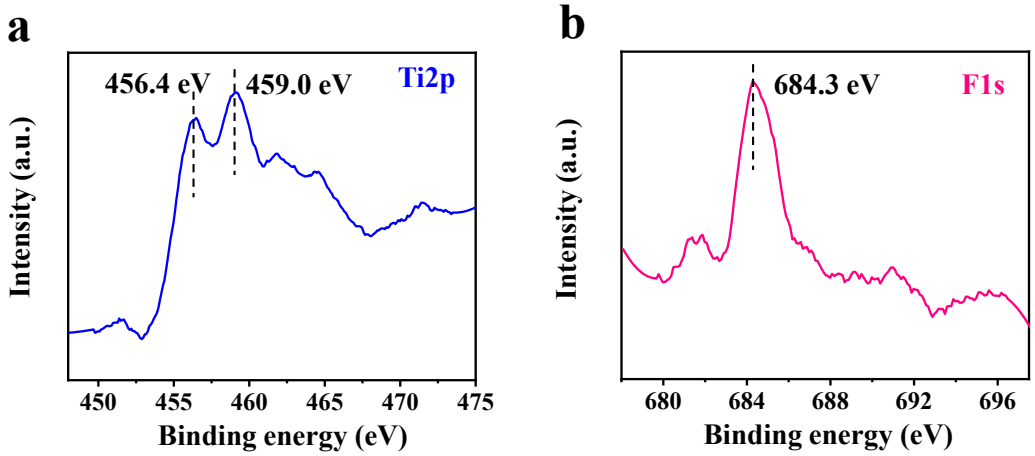

Fig. S6. (a) XPS wide scan of the prepared rGO and rGO/MXene heterogeneous membranes. (b) XPS spectra of the rGO and rGO/MXene heterogeneous membranes for Ti2p core level.

Table S1. Element composition of rGO and rGO/MXene heterogeneous membranes.

Membranes	**Element composition(wt%)**			
	C1s **(284.8 eV)**	O1s **(532.7 eV)**	Ti **(455.5 eV)**	**F (685.0 eV)**
rGO	68.24	31.76	/	/
rGO/MXene	67.18	30.72	1.08	1.01

Table S2. Normalized areas of characteristic peaks in the C1s XPS spectra of rGO, and rGO/MXene heterogeneous membranes.

Membranes	Functional group composition				
	C=C/C-C(%)	C-O /C-O-C(%)	C=O (%)	C-Ti (%)	-COOH (%)
rGO	76.98	16.52	4.16	/	2.34
rGO/MXene	46.46	34.63	11.64	5.85	1.43

Table S3. XPS Element composition with different etch depth of rGO/MXene heterogeneous membranes

Etch depth (nm)	Element composition			
	C (at.%)	O (at.%)	Ti (at.%)	F (at.%)
0	67.18	30.72	1.08	1.01
1.15	76.24	20.03	2.1	1.63
2.30	78.03	17.99	2.43	1.55

PS. 7 XRD patterns of MXene heterogeneous membranes.

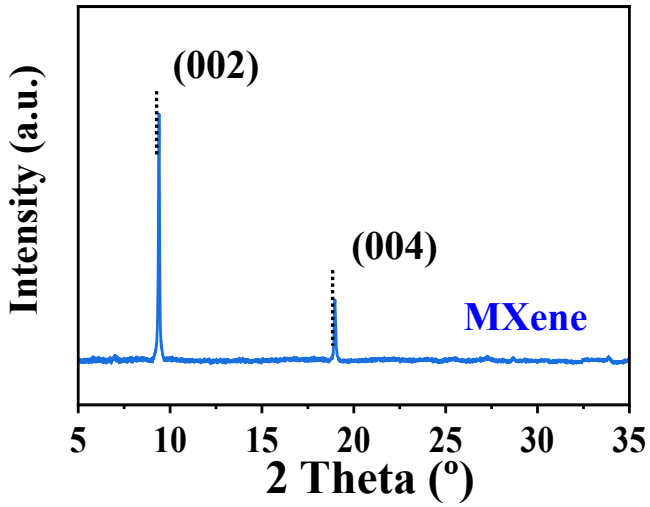

Fig. S7. XRD patterns of MXene heterogeneous membranes.

PS. 8 The TGA curves of rGO membranes and rGO/MXene heterogeneous membranes

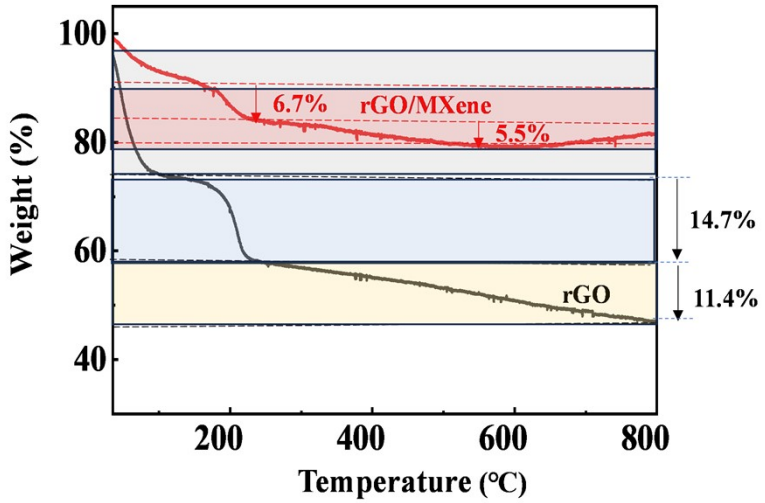

Fig. S8. The TGA curves of rGO membranes and rGO/MXene heterogeneous membranes.

PS. 9 The adsorption experiment for rGO/MXene heterogeneous membrane in 10 mg L^{-1} MB solution.

We have further analyzed the dye adsorption performance of the rGO/MXene heterogeneous membranes. In details, after rGO/MXene membranes were prepared using vacuum filtration, 300 mL 10 mg L^{-1} MB solutions were added to the feed side. The dyes solution was stirred with a blender at ~180 rpm without filtration. Afterwards, the samples solutions were collected at pre-determined time intervals in 120 min, and analyzed for residual MB concentrations. Due to the MB solutions own gravity, the filtrates were collected only ~2 mL after 120 min. A small amount of filtrates solution has negligible effect on the concentration of the dyes during the adsorption experiments.

The adsorption efficiency (AE) was calculated by using the following expression (1) :

$$AE=\left(1-\frac{C_a}{C_0}\right)*100\% \qquad (1)$$

where C_o and Ca (mg L^{-1}) are initial and final solution concentrations after adsorption equilibrium, respectively;

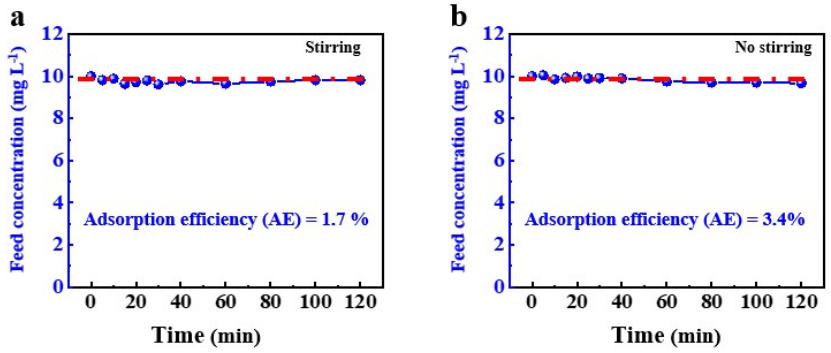

Fig. S9. The adsorption experiment for rGO/MXene heterogeneous membrane in 10 mg L^{-1} MB solution with stirring (a) and without stirring (b).

PS. 10 Effects of different MXene ratios on performances of rGO/MXene heterogeneous membranes

Table S4. Element composition of rGO and rGO/MXene heterogeneous membrane.

Membranes	Element composition(wt%)			
	C1s **(284.8 eV)**	O1s **(532.7 eV)**	Ti (**455.5 eV**)	**F(685.0 eV)**
rGO/MXene(3:1)	67.24	31.68	0.50	0.58
rGO/MXene(2:1)	65.44	33.15	0.76	0.65
rGO/MXene(1:1)	67.18	30.72	1.08	1.01
rGO/MXene(1:2)	66.68	30.4	1.51	1.41
rGO/MXene(1:3)	63.86	33.05	1.97	1.12

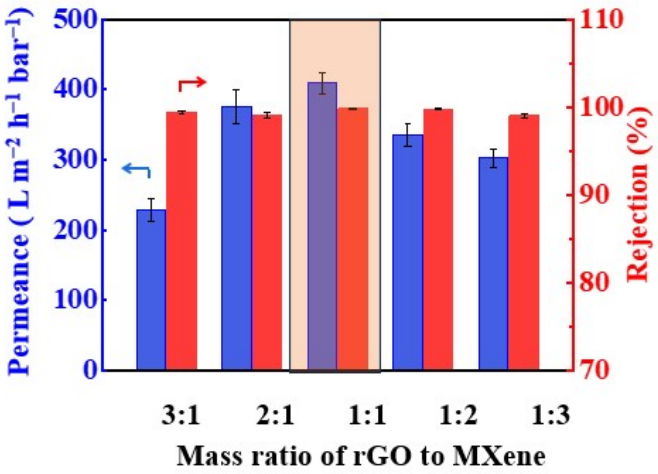

Fig. S10. Water permeability and MB solution rejection of rGO/MXene heterogeneous membrane with varying MXene ratios.

PS. 11 Comparisons of water permeance and rejection for dyes of rGO/MXene heterogeneous membranes in this work with other NF membranes in literatures

Table S5. Comparisons of water permeance and rejection for dyes of rGO/MXene heterogeneous membrane in this work with other NF membranes in literatures

Type	Membrane	Rejection (%)	Permeance (L h^{-1} m^{-2} bar^{-1})	References
GO-Based membrane	C-GO/PAN	>99	78.5-117.2	(6)
	GO/COF	92.01	119	(7)
	GO	98.1	20	(8)
	ZnO/rGO	98	225	(8)
	ZIF-8@GO	99.8	49.8	(9)
	UiO-66-rGO	95	30.6	(10)
	GO-CNTs	99.3	7.2	(11)
	GO-CTF_5	93.8	226.3	(12)
	GO/P25	98.1	5.8	(13)
	COF@GO-50	99.0	135.7	(14)
	C-BCGO-Au stc-M	24.4	32.4	(15)
	carboxyl pillararenes (CP6)-GO	98	119	(16)
	MIL-100(Fe)@GO (MGO) membrane	98.8	89.4	(17)
	OE/GO composite membrane	~100	165	(18)
	GO/TANT	93	300	(19)
	PPy/GO membrane	96	310	(20)

	GO/MXene	99.5	71.9	(21)
	GO/MXene	99	79.58	(22)
	S-rGO	99.9	236.2	(23)
	GO/HTGO	77.7	99.96	(24)
Other 2D material membrane	PAA-MXene/PAN	98.9	271.3	(25)
	CA-Ti_3C_2Tx composite membrane	98.2	100.0	(26)
	Hybrid lignin-intercalated MXene membranes	95	61.22	(27)
Polymeric membrane	Sepro NF 2A	4.8	99.9	(28)
	Su/TMC	99.4	52.4	(29)
	β-cyclodextrin	96.4	179.93	(30)
	Arg/TMC membrane	99.6	130	(31)
	ML-based membranes	98	104.9	(32)
	NGQDs-CD-MWCNTs-5	99	12.35	(33)
	β-CD/APPD/P84 membranes	98.67	105	(34)
	Cu-TpPa/HPAN membranes	99	92.1	(35)
This Work	rGO/MXene	99.7	401.2	*

PS. 12 Stability of the rGO membranes and rGO/MXene heterogeneous membrane of stirred effect.

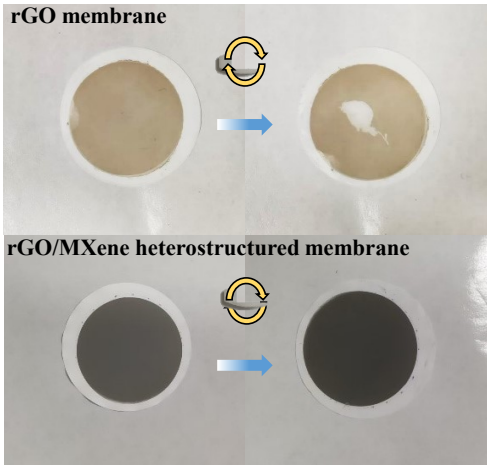

Fig. S11. Stability of the rGO membranes and rGO/MXene heterogeneous membrane of stirred effect.

PS. 13 The digital image of dead- end pressure filtration cell.

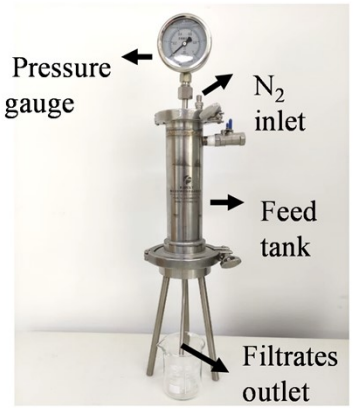

Fig. S12. The digital image of dead- end pressure filtration cell.

PS 14 Comparison of the nanofiltration performance of the rGO/MXene heterogeneous membranes for 10 mg L^{-1} MB solution before and after 50 deformation cycles .

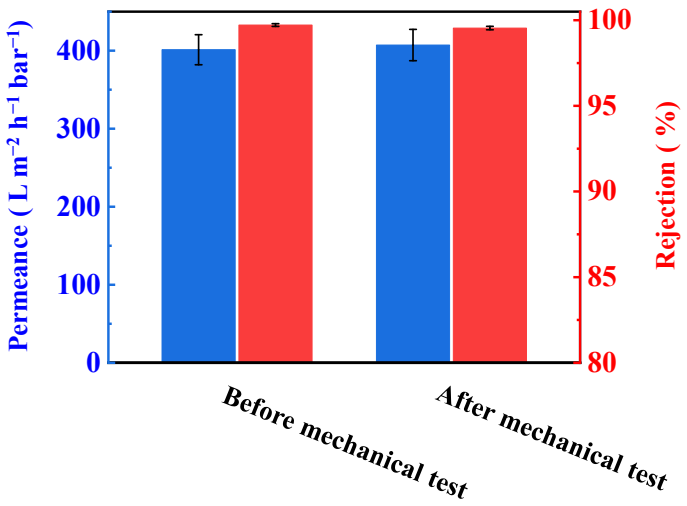

Fig. S13. Comparison of the nanofiltration performance of the rGO/MXene heterogeneous membranes for 10 mg L^{-1} MB solution before and after 50 deformation cycles.

PS. 15 The comparison of tensile strength and elongation of rGO and rGO/MXene heterogeneous membranes.

Table S6. The comparison of tensile strength and elongation of rGO and rGO/MXene heterogeneous membranes.

Membranes	**Tensile strength(Mpa)**	**Elongation(%)**
rGO	5.54	11.92
rGO/MXene	7.63	3.47

PS. 16. The stability of rGO/MXene heterogeneous membrane under harsh conditions.

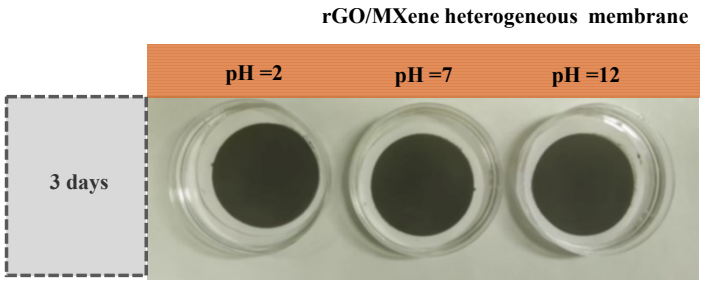

Fig. S14. Digital photos of the rGO/MXene heterogeneous membrane immersed in acidic, neutral, and alkaline water for a 3 days long duration.

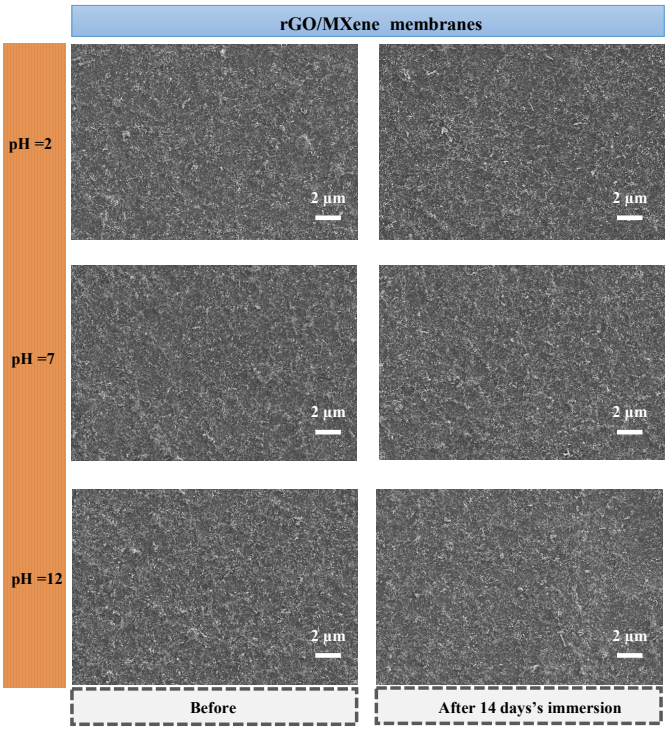

Fig. S15. SEM images of the rGO/MXene membrane before and after treatment in different chemical environments

PS. 17 Thickness-Dependent MB rejection in 2D rGO/MXene heterogeneous lamellae membrane

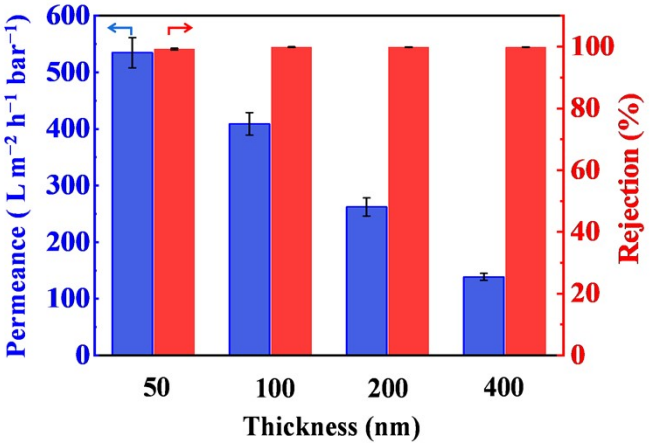

Fig. S16. Thickness-dependent MB rejection in 2D rGO/MXene heterogeneous lamellae membrane.

PS. 18 Structural properties of dye molecules

Table S7. List of the dye solutes used in this work.

Type	Chemcial Structure	Approximate Size (nm)	Molecular Weight (g mol^{-1})
Methylene Blue (MB)	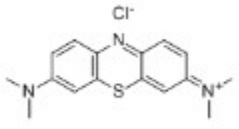	0.5 *0.7 * 1.4 nm	319.85
Rhodamine B (RB)	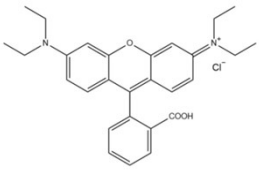	~1.20 nm	479.01
Pararosaniline (PA)	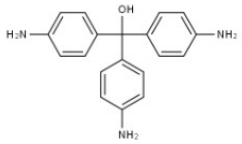	~1.02 nm	287.36
Congo Red (CR)	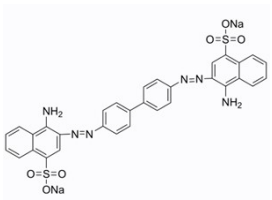	0.7 * 2.5nm	696.66

PS. 19 Performances of rGO/MXene heterogeneous membrane for rejecting different dyes

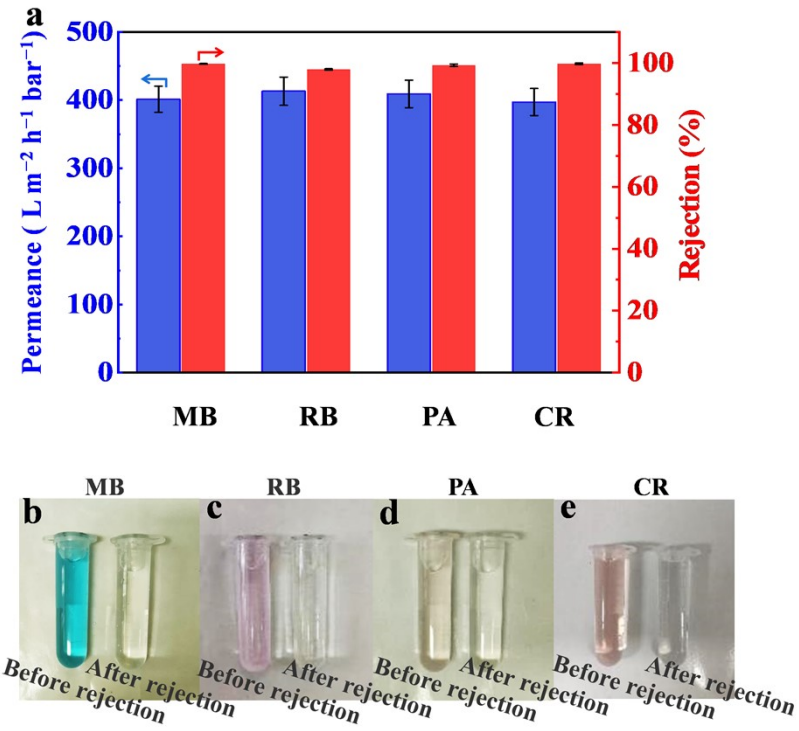

Fig. S17. (a) Separation performance of rGO/MXene heterogeneous membrane for a range of dyes molecules. Photos of filtrate and feed solution of rGO/MXene heterogeneous membranes for rejecting (b) MB, (c) Rb, (d) PA, and (e) CR solutions.

PS. 20 The anti-fouling performance test of rGO/MXene heterogeneous membranes.

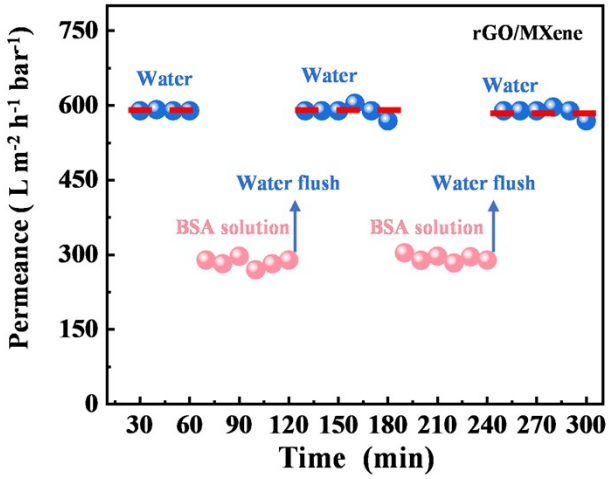

Fig. S18. The anti-fouling performance test of rGO/MXene heterogeneous membranes.

PS. 21 Density functional theory calculations

We also performed Density Functional Theory (DFT) calculations to illustrate the underlying physical mechanism of the enhanced water flux for rGO/MXene heterogeneous membranes. The rGO was constructed by hydroxyl-functionalized graphene, while MXene was modeled using fluorine-terminated $Ti_3C_2F_2$ (Fig. S19a-c). The selection of this model is consistent with our experimental XPS observations. Owing to the hydrogen bonding interactions, the adsorption energy (E_{ad}) between water molecule and rGO sheet (water-rGO) is -7.36 kcal mol^{-1}. In contrast, E_{ad} between water molecule and fluorine-terminated MXene sheet is -3.37 kcal mol^{-1}, which is less than half of that for rGO. This weak adsorption between water and MXene sheet leads to the high-velocity water transport on MXene, and thus resulting the highwater flux for rGO/MXene heterogeneous membranes.

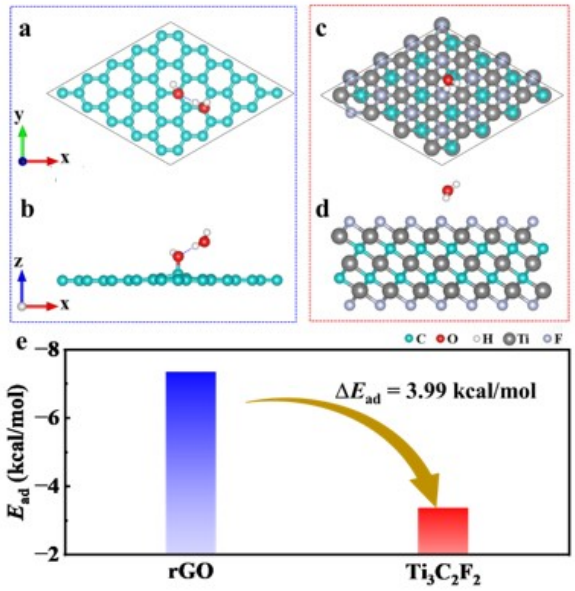

Fig. S19. Adsorption mechanism of water molecule on rGO and MXene $Ti_3C_2F_2$. (**a, b**) Top and side views of the optimized geometric configuration of a water molecule adsorption on the hydroxyl-functionalized rGO. (**c, d**) Top and side views of a water molecule on the fluorine-terminated MXene ($Ti_3C_2F_2$). The green, red, white, grey, and silver spheres represent C, O, H, Ti, and F atoms, respectively. The blue dashed lines denote the hydrogen bonds formed at the interface. (**e**) Adsorption energy (E_{ad}) of H_2O on rGO and $Ti_3C_2F_2$, respectively.

References

(S1)G. Kresse and J. Furthmüller, *Phys. Rev. B*, 1996, **54**, 11169-11186.

(S2) G. Kresse and D. Joubert, *Phys. Rev. B*, 1999, **59**, 1758-1775.

(S3)J. P. Perdew, K. Burke and M. Ernzerhof, *Phys. Rev. Lett.*, 1996, **77**, 3865-3868.

(S4)S. Grimme, J. Antony, S. Ehrlich and H. Krieg, *J. Chem. Phys.*, 2010, **132**, 154104.

(S5)H. J. Monkhorst and J. D. Pack, *Phys. Rev. B*, 1976, **13**, 5188-5192.

(S6) C. Xing, J. Han, X. Pei, Y. Zhang, J. He, R. Huang, S. Li, C. Liu, C. Lai, L. Shen, A. K. Nanjundan and S. Zhang, *ACS Appl. Mater. Interfaces*, 2021, **13**, 55339-55348.

(S7) L. Chen, W. Wang, Q. Fang, K. Zuo, G. Hou, Q. Ai, Q. Li, L. Ci and J. Lou, *Appl. Mater. Today*, 2020, **20**, 100791.

(S8) W. Zhang, H. Xu, F. Xie, X. Ma, B. Niu, M. Chen, H. Zhang, Y. Zhang and D. Long, *Nat. Commun.*, 2022, **13**, 471.

(S9) W. H. Zhang, M. J. Yin, Q. Zhao, C. G. Jin, N. Wang, S. Ji, C. L. Ritt, M. Elimelech and Q. F. An, *Nat. Nanotechnol.*, 2021, **16**, 337-343.

(S10) K. Guan, D. Zhao, M. Zhang, J. Shen, G. Zhou, G. Liu and W. Jin, *J. Membr. Sci.*, 2017, **542**, 41-51.

(S11) H. Kang, J. Shi, L. Liu, M. Shan, Z. Xu, N. Li, J. Li, H. Lv, X. Qian and L. Zhao, *Appl. Surf. Sci.*, 2018, **428**, 990-999.

(S12) N. A. Khan, J. Yuan, H. Wu, L. Cao, R. Zhang, Y. Liu, L. Li, A. U. Rahman, R. Kasher and Z. Jiang, *ACS Appl. Mater. Interfaces*, 2019, **11**, 28978-28986.

(S13) C. Xu, Y. Xu and J. Zhu, *ACS Appl. Mater. Interfaces*, 2014, **6**, 16117-16123.

(S14) R. Ge, T. Huo, M. X. Nie, J. Lu, H. Hou and X. Zhan, *Sep. Purif. Technol.*, 2025, **355**, 129637.

(S15) Y. Zhong, S. Mahmud, Z. He, Y. Yang, Z. Zhang, F. Guo, Z. Chen, Z. Xiong and Y. Zhao, *J. Hazard. Mater.*, 2020, **397**, 122774.

(S16) X. Ding, M. Nie, S. Cheng, R. Li, Y. Wang, A. S. Ali, X. Han and Y. Sun, *Sep. Purif. Technol.*, 2025, **365**, 132667.

(S17) Y.-H. Ren, W.-H. Zhang, M.-J. Yin, Z.-J. Liu and Q.-F. An, *Desalination*, 2025, **613**, 119001.

(S18) H. Mushtaq, M. M. ur Rehman, A. Shaheen, M. A. Rashid, K. H. Thebo and J. Akhtar, *Fuller. Nanotub. Car. N.*, 2025, 1-10.

(S19) Y. Zhang, P. Qi, H. Zuo, Y. Jin, S. Li, Y. Hu and G. Gong, *Chem. Eng. J.*, 2025, **522**, 167843.

(S20) T. Zhang, Z. Huang, D. Cui, Z. Luo, X. Zhuo, Y. Liu, X. Wang, K. Wu, J. Zhang, G. Li, S. Sun, H. Zuilhof and H. Lu, *J. Membr. Sci.*, 2025, **735**, 124602.

(S21) T. Liu, X. Liu, N. Graham, W. Yu and K. Sun, *J. Membr. Sci.*, 2020, **593**, 117431.
(S22) D. Yu, L. Sun, Y. Zhang, Y. Song, C. Jia, Y. Wang, Y. Wang, M. J. Kipper, J. Tang and L. Huang, *Chem. Eng. J.*, 2024, **480**, 148009.
(S23) L. Yan, J. Chen, Z. Zhang, Z. Liu, T. Ding and G. Shi, *J. Hazard. Mater.*, 2025, **487**, 137078.
(S24) B. Xie, M. Huang, Y. Fan, J. Lan, F. Zhou, J. Chen and L. Chen, *Sep. Purif. Technol.*, 2026, **385**. *136294*
(S25) Y. Zhang, S. Li, R. Huang, J. He, Y. Sun, Y. Qin and L. Shen, *J. Membr. Sci.*, 2022, **648**, 120360.
(S26) Y. Zhao, M. Wei, Y. Wang, Y. Zhang, J. Liu, H. Zhang, D. Chen, J. Wang and L. Wang, *J. Alloys Compd.*, 2025, **1036**, 181847.
(S27) X. Zhang, S. Cheng, R. Li, Z. Guo, Y. Zhao, Y. Sun, Y. Chen, L. Nie and Z. Li, *Sep. Purif. Technol.*, 2025, **376**, 134122.
(S28) J. Lin, W. Ye, H. Zeng, H. Yang, J. Shen, S. Darvishmanesh, P. Luis, A. Sotto and B. Van der Bruggen, *J. Membr. Sci.*, 2015, **477**, 183-193.
(S29) P. Jin, S. Chergaoui, J. Zheng, A. Volodine, X. Zhang, Z. Liu, P. Luis and B. Van der Bruggen, *J. Hazard. Mater.*, 2022, **421**, 126716.
(S30) J. Li, J.-L. Gong, G.-M. Zeng, B. Song, W.-C. Cao, S.-Y. Fang, S.-Q. Tang, Y. Guan, Z.-K. Tan, Z.-P. Chen, X.-Q. Mao and R.-L. Zhu, *Sep. Purif. Technol.*, 2021, **276**, 119352.
(S31) R. Zhao, P. Jin, J. Zhu, Y. Li, G. Li, A. Volodine, Y. Liu, J. Zheng and B. Van der Bruggen, *J. Membr. Sci.*, 2023, **673**, 121477.
(S32) X. Zhu, H. Qiu, W. Yan, Z. Sun, X. Kang, J. Xu, D. Wu, H. Liang, X. Cheng and D. Xu, *Desalination*, 2024, **586**, 117851.
(S33) J. Li, J.-L. Gong, S.-Y. Fang, W.-C. Cao, S.-Q. Tang, M. Qin, H.-Y. Zhou and Y.-W. Wang, *J. Colloid Interface Sci.*, 2023, **641**, 197-214.
(S34) Z. G. Abdi, J.-Y. Lai and T.-S. Chung, *Desalination*, 2023, **549**, 116365.
(S35) Y. Zhang, S. Tian, Q. Sha, T. Yang, Y. Huang, X. Zhang, W. Wang and N. Han, *J. Membr. Sci.*, 2024, **705**, 122907.